Water Supply

Water Supply Vol 22 No 1, 990 doi: 10.2166/ws.2021.220

Vibration characteristics of pressure pipelines at pumping stations and optimized design for vibration attenuation

Yude Xu[a], Zijin Liu[a,b,*], Dongmeng Zhou[a,b], Junjiao Tian[a,b] and Xinglin Zhu[a,b]

[a] School of Water Conservancy, North China University of Water Resources and Electric Power, Zhengzhou 450046, China
[b] Henan Provincial Hydraulic Structure Safety Engineering Research Center, Zhengzhou 450046, China
*Corresponding author. E-mail: 1556135694@qq.com

ABSTRACT

To explore the effects of different pressure pipeline layouts on pumping station pipeline vibration, this study establishes an ALGOR numerical model for pipeline flow considering fluid–structure interactions. A data acquisition and signal processing vibration test system is used to obtain vibration signals and verify simulation results including pipeline fluid velocity, fluid pressure, and transient stress. Based on the flow's vibration excitation characteristics, we consider structural vibration reduction technology and propose an optimized design scheme. As an example, we apply this approach to a pressure pipeline at the Ningxia Yanhuanding Pumping Station Project. Results show strong vibrations at the water inlet, the junction between the branch and main pipes, and the water outlet, with even stronger vibration at the inlet than at the outlet. In the optimized design scheme, adjusting the distance between the branch pipes only weakly reduces flow-generated pipeline vibration; increasing the pipe diameter and changing the main pipe's relative orientation show stronger effects. Vibration reduction is optimized for a main pipe dip angle of 2–5° relative to the branch pipes, simultaneously decreasing pumping station energy loss. These results provide a theoretical and practical basis for optimal design of pressure pipelines at high-lift pumping stations.

Key words: ALGOR numerical model, modal analysis, optimization scheme, pressure pipeline, pump stations, vibrations

HIGHLIGHT

- This paper established fluid-structure interaction-based water flow ALGOR numerical model of pressure pipeline in a pump station; meanwhile, DASP vibration test system is adopted to acquire the vibration signals to verify the simulation results, analyze the incentive characteristics of pressure pipeline flow formed on pipeline vibration and put forward an optimized design scheme.

INTRODUCTION

Pipelines at high-lift pumping stations may exhibit vibrations arising from high-pressure water delivery, significantly degrading operational safety and pumping station structural service life. Such pressure pipelines are typically composed of concrete or steel pipes. Altered pipe size or elbow layout could restrict water flow, causing flow rate and pressure intensity variations. In turn, unsteady flow could further expose the pipeline to the fluid's dynamic pressure, causing pipeline vibrations. Not only can this damage a pressure pipeline, but it also increases its resistance loss, decreasing water delivery efficiency and increasing energy consumption in irrigation pumping (Madzivire *et al.* 2019).

The pipeline vibration problem has been studied by scholars worldwide over many years, yielding significant progress. In the 1970s, this research achieved a breakthrough and entered a practical stage with the help of computers (Bu 2006). Among studies of nonlinear vibration in fluid-conveying pipelines, Jin and Zou (Jin 1997; Jin & Zou 2003) found that large flow velocity and small elastic support stiffness may result in fluttering, dynamic instability, and even chaotic motion of a cantilever DC pipeline. In a gas–liquid two-phase flow pipeline system, the exciting force often occurs at fluid turning points such as bends, elbows, and T-joints (Wang 2006; Zeng 2007). Hara (1975, 1980) studied pipeline vibration caused by two-phase flow, derived the equation of motion for free vibration of two-phase flow pipelines, and pointed out that pipeline vibration is mainly caused by the centrifugal force and changes in the quality of the vibrating system. Keramat *et al.* (Keramat & Ahmadi 2012; Keramat *et al.* 2012; Zanganeh *et al.* 2015) theoretically and experimentally analyzed pipeline vibration and studied fluid–structure interaction with viscoelastic supports under the action of water hammer. Ahmadi & Keramat

(2010) explored the node-coupling effect using finite-element-based structural and hydraulic equations to study water hammer with fluid-structure interactions. Many of the above-mentioned studies are mostly theoretical, cursory, or experimental. In practice, various potentially problematic factors must be considered comprehensively and solved with reference to previous research. However, few studies have considered the vibration of pressure pipelines at pumping stations. Moreover, because pressure pipeline structures take diverse forms, governments have not generally established a unified evaluation standard for vibration performance in this context. Therefore, it is difficult to evaluate pipeline vibration. Interactions between fluids and structures (fluid–structure interactions) are common in fields such as ocean engineering, shipping, aviation, water conservancy, chemical engineering, and nuclear power. Dynamic analysis of fluid–structure interactions has been reported in a wide array studies using analytical, semi-analytical, or numerical methods. Among these, the finite-element-based numerical method is used most often because it considers three-dimensional nonlinear effects. Alternatively, the integral solution method or the alternate solution method can be used to solve the problem. The activation likelihood estimation (ALE) method (Meng *et al.* 2010) is effective, but the grid movement it describes often relies on simplifications. In particular, it cannot treat cases wherein the boundaries of the fluid domain change drastically, so certain problems must be solved before using ALE. Examples include effectively describing the nonlinearity of the coupling interface, separating node pairs, and transmitting the resulting coupled physical quantities. Previous research revealed the principles of pipeline vibration, laying a foundation for the study of fluid–structure interaction. Flow-excited vibration in pipeline structures and optimizing vibration reduction remain topics requiring further study. With the rapid development of fluid–structure interaction theory and simulation software, simulations can now reliably represent pipeline vibration. In 2004, Ying Huaiqiao and Liu Jinming and coworkers at the China Orient Institute of Noise & Vibration developed data acquisition and signal processing (DASP) software based on time-domain analysis of vibration modes. Their approach can simultaneously identify multi-order, closely spaced modes without applying a known excitation force, showing apparent advantages (Xie & Xue 2006) in efficiency and accuracy compared with frequency-domain mode analysis.

Building on prior research to address the above-mentioned literature gaps, this study establishes a fluid–structure interaction (FSI) finite-element numerical model based using ALGOR software. The model is then used to analyze hydrodynamic pipeline vibration response through pipe flow state analysis and model identification. As a real-world application, pressure pipeline No. 1 for Pumping Station No. 2 at the Ningxia Yanhuanding Pumping Station Project (Phase I) is treated with the proposed model. In addition, a DASP vibration test system is adopted to capture and verify vibration signals in order to characterize the influence of water flow on the pipeline's vibration modes. Based on the results, an optimized design scheme is proposed.

METHODS

Simulation principle and method

ALGOR is a well-known, large-scale, general-purpose finite-element simulation software. It is very popular with workers engaged in design analysis because of its complete functions, ease of use, and modest hardware requirements. Consequently, it has been widely used in design, finite-element analysis, and mechanical motion simulation in various industries. ALGOR software can easily and quickly perform design analysis in many kinds of problems: static, dynamic, linear, nonlinear, heat conduction, flow fields, electric fields, pipeline processes, and multi-physics coupling. Time- and cost-effective, it can predict and verify various real-world conditions and complete design projects. Vibration and flow characteristics of flow-induced pressure pipelines have been examined previously (Tan *et al.* 2006). The present study adopts the ALGOR finite-element simulation model to analyze the natural vibration characteristics of pressure pipelines. We simulate the stress and strain resulting from FSI in an operating water pressure pipeline. When vibration occurs in a pressure pipeline, there is a mutual interaction between the fluid and the solid pipeline, changing the pipeline's state of motion. Therefore, to study pipeline vibration, it is necessary to conduct FSI analysis on both the pipeline and the fluid. Fluid motion within the pipeline interacts with the solid pipeline interface, which also changes the pipeline's state of motion. The FSI governing equations are described as follows.

Fluid governing equation

Fluid motion follows three basic physical laws of conservation (Ozdemir *et al.* 2010):

Mass conservation:

$$\frac{\partial \rho_f}{\partial t} + \nabla \cdot (\rho_f v) = 0 \tag{1}$$

Momentum conservation:

$$\frac{\partial \rho_f v}{\partial t} + \nabla \cdot (\rho_f v \cdot v - \tau_f) = f_f \tag{2}$$

Energy conservation:

$$\frac{\partial (\rho h_{tot})}{\partial t} - \frac{\partial p}{\partial t} + \nabla \cdot (\rho_f v h_{tot}) = \nabla \cdot (\lambda \nabla T) + \nabla \cdot (v \cdot t) + v \cdot \rho f_f + S_E \tag{3}$$

Here, t is time; f_f is the body force vector; ρ_f is the fluid density; v is the fluid velocity vector; τ_f is the shear force tensor; λ is the thermal conductivity coefficient; and S_E is the energy source term. In turn, τ_f can be expressed as

$$\tau_f = (-p + \mu \nabla \cdot v) I + 2\mu e \tag{4}$$

where p is the fluid pressure; μ is the dynamic viscosity; and e is the velocity stress tensor, $e = \frac{1}{2}(\nabla v + \nabla v^T)$.

Solid control equation

The conservation equation for the system's solid component is deduced from Newton's second law:

$$\rho_s \ddot{d}_s = \nabla \cdot \sigma_s + f_s \tag{5}$$

The thermal deformation caused by temperature differences is

$$f_T = \alpha_T \cdot \Delta T \tag{6}$$

where ρ_s is the solid density; σ_s is the Cauchy stress tensor; f_s is the body force vector; $\ddot{d}_s$ is the local acceleration vector of the solid domain, α_T is the temperature-related thermal expansion coefficient, and ΔT is the temperature difference.

Fluid-structure interaction equation

FSIs follow the most basic conservation law. The basic governing equation adopted in FSI analysis is expressed as (Wang & Wei 2009):

$$\begin{cases} \tau_f \cdot n_f = \tau_s \cdot n_s \\ d_f = d_s \\ q_f = q_s \\ T_f = T_s \end{cases} \tag{7}$$

where f denotes the fluid region; s denotes the solid region; τ is the solid stress; d is the displacement; q is the heat flux; and T is the temperature.

ALGOR fluid field analysis equation

ALGOR fluid analysis adopts the Navier–Stokes equation, which describes viscous Newtonian fluids:

$$\rho\left(\frac{\delta u}{\delta t} + u \nabla u\right) + \nabla p - \mu \nabla^2 u = 0 \tag{8}$$

Here, ρ is the fluid density; u is the velocity component of the fluid at time t; p is the fluid pressure; and t is time.

Basic process analysis based on finite-element analysis

The proposed method of analysis proceeds in several stages. The preparation stage consists of:

(1) Pretreatment: 3D modeling, setting material properties, and parameter definition.
(2) Solving: In the modal solution, nonlinear structures may also be solved as linear structures.
(3) Post-processing: Structural graphics display the modal calculation and analysis results.

In this study, we used ALGOR software to perform finite-element analysis considering FSI. The basic processes are described below.

Fluid analysis:

(1) Import a 3D pressure pipeline model, set the pipeline as being filled with water using ALGOR software, and mesh the pipeline and water domains simultaneously. The water grid requires tetrahedral and wedge-shaped mesh elements. Through mesh division, the overall structural model is discretized into finite elements. The elements are connected in the form of nodes to construct an element stiffness matrix. Finally, a finite-element equation is established.
(2) Simulate water characteristics using ALGOR's flow field analysis function, specify simulation boundary conditions, and calculate flow behavior based on the internal fluid model.
(3) Obtain the flow rate and pressure.

Natural modal analysis:

(1) Copy the fluid analysis model, disable the fluid in the pressure pipeline, and retain the empty pressure pipe model.
(2) Perform natural modal analysis of the structure to obtain its natural frequency and the first six orders of vibration modes.

Transient stress analysis:

(1) Based on the pipeline's modal analysis results, use the fluid analysis flow rate and pressure results to apply an external load.
(2) Calculate the pipeline structure's transient stress arising from the flow from start-up to stable operation.

Project example

ALGOR fluid field analysis equation

Considering the No. 1 pressure pipeline at the second pumping station of the Ningxia Yanhuanding Pumping Station Project as a test case, an ALGOR FSI finite-element model was established to analyze the hydrodynamic response to pipeline vibrations. According to field studies, inlet pipes 4 and 8 have suffered long-term vibration during operation, seriously affecting the pumping station's safe operation. Additionally, the layout presents typical multi-machine, single-pipe characteristics. Therefore, this pressure pipeline was selected as the subject of study.

The piping layout is shown in a plan view in Figure 1(a). The No. 1 pressure pipeline consists of right and left inlet branch pipes and a main outlet pipe. Pipes ① and ② have inner diameters of 1.00 m and 0.80 m, respectively; pipe ③ has inner diameters of 1.00 m and 1.40 m at its left and right ends, respectively. At the elbow, it has outer and inner diameters of 2.50 m and 1.50 m, respectively, and an axis radius of 2.00 m. Pipe ④ has an inner diameter of 1.40 mm. The wall thickness of all pipes is 12 mm. As for material parameters, the pipeline is considered as a simplified steel pressure pipe of homogeneous material with a density of 7.85 g/cm^3, an elastic modulus of 2.06×10^5 MPa, and a Poisson's ratio of 0.3.

Simulated conditions

Given the actual vibration of pumps No. 4 and No. 8, which share the No. 1 pressure pipeline, the following two representative working conditions were selected for flow regime simulations:

(1) Working condition 1: The No. 4 pump operates normally and the No. 8 pump is stopped.
(2) Working condition 2: Both pumps No. 4 and No. 8 operate normally.

Boundary conditions and mesh generation

The steel pressure pipeline's calculated Reynolds number exceeded 2,300; therefore, the standard k–ε turbulence model was used. The inlet boundary condition set the velocity V_{in} in both branch pipes according to the section average flow rate, and the outlet boundary conditions were set as free flows. The pipe wall used non-slip boundary conditions, and the fluid surface within the pipe

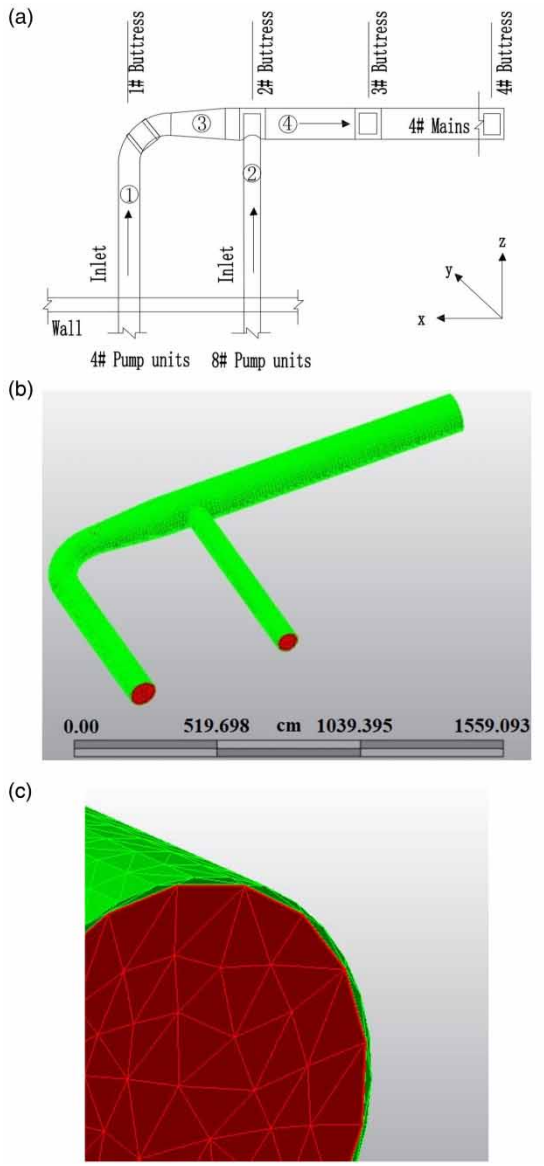

Figure 1 | (a) Schematic diagram of the pressure pipeline layout of Phase I's No. 2 pumping station; No. 1 pressure pipeline model mesh illustration showing (b) the integral structure and (c) a detail view.

was free. At working condition 1, machine No. 4 had a rated inlet flow of 2 m^3/s and an inlet flow velocity of 2 m/s while the No. 8 machine had a flow velocity of zero. At working condition 2, the inlet boundary flow rate of pump No. 8 was 2.5 m/s.

The domains of both the pressure pipeline and the water volume inside it were meshed within the ALGOR environment. A grid comprising both tetrahedral and wedge-shaped elements was used at the water inlet and in the main outlet pipe. A hybrid grid was adopted in the elbow and in the joint between the main pipe and the branch pipe; these regions were assigned higher grid density. For meshing details, see Figure 1(b) and 1(c).

RESULTS AND DISCUSSION

Pipeline hydrodynamic analysis

The period of the first 120 s after starting up, during which the pipeline flow is stable, was selected as a typical period for transient flow analysis. The flow velocity, flow pressure, and transient stress in the pressure pipeline were calculated under working conditions 1 and 2; results are shown in Figures 2 and 3, respectively.

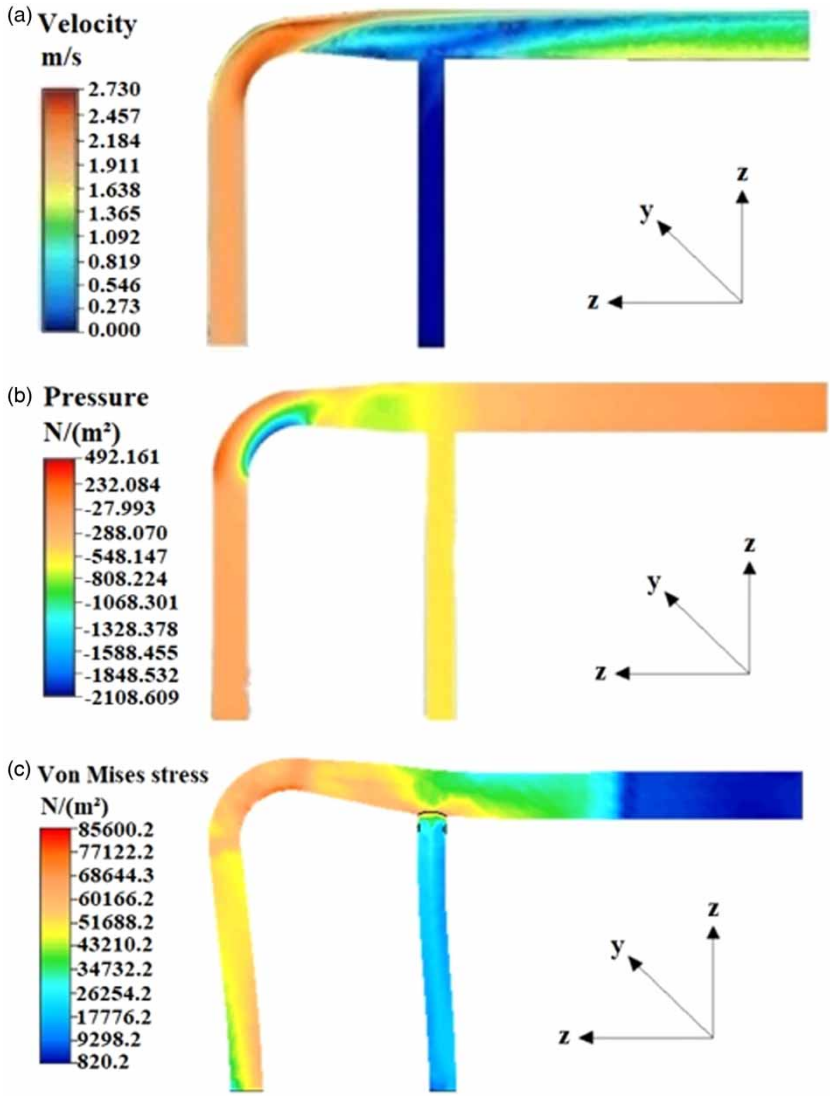

Figure 2 | Distributions of pipeline (a) flow velocity, (b) pressure, and (c) transient stress at 120 s in working condition I.

Working condition 1

Calculation results for the 120-s transient flow velocity, pressure intensity, and transient stress distribution at section XY are shown in Figure 2(a)–2(c). Figure 2(a) shows that, during steady main pipe discharge, pump No. 4 maintained a large inlet flow rate with a maximum at the elbow. In addition, the chain relative ratio of flow velocity within the elbow was large and four-level flow velocities occurred there, readily causing backflow and low pressure. This causes increased flow resistance and unsteady, rough flow at the elbow. Pump No. 8's inlet pipe was filled with water but the flow rate was zero and the pressure was distributed evenly. 44 s later, a clear low-flow-rate zone appeared at the main outlet pipe's No. 2 buttress. The back-end flow velocity increased gradually, but flow levels were distributed unevenly with disordered flow regimes. 60 s later, the main outlet pipe's pressure intensity increased gradually and pressure was mainly evenly distributed at pump No. 4's inlet pipe and at the main outlet pipe.

In general, when only pump No. 4 operated, the inlet flow velocity was large and unevenly distributed. Changes in hydraulic pressure may stimulate pipeline vibration. The flow velocity at the elbow changed significantly, generating a negative pressure zone and thus increasing the impact of the flow on the elbow. The uneven flow velocity in the main outlet pipe and the low-velocity zone caused unstable flow and large changes in pressure. Hence, the flow in the main outlet pipe generated strong pipeline excitation, causing vibration. However, pump No. 8's inlet flow exerted no pipeline excitation.

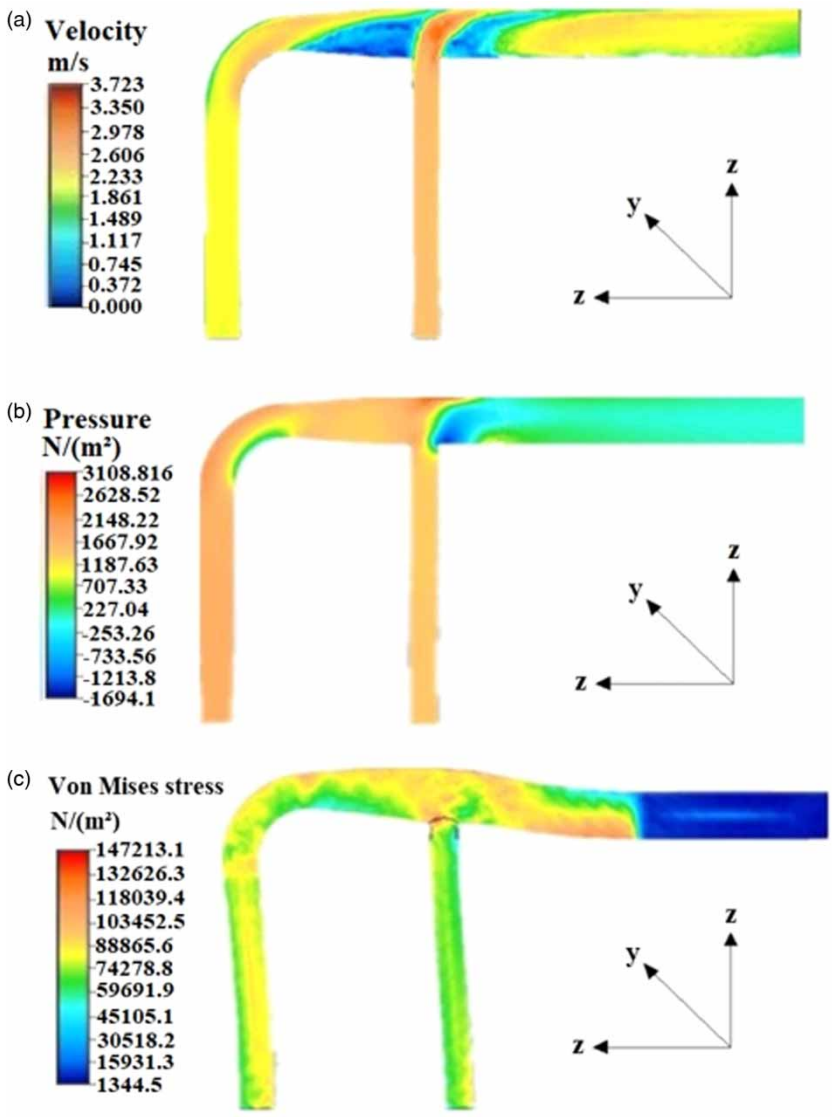

Figure 3 | Distributions of pipeline (a) flow velocity, (b) pressure, and (c) transient stress at 120 s in working condition II.

Therefore, during start-up of pump No. 4, flow impact and uneven flow velocity, water pressure, and transient stress were the main causes of unsteady main pipe flow. The inlet pipe and the No. 1 and No. 2 anchor blocks of pump No. 4 were easily excited by the flow and caused shock excitation, necessitating vibration attenuation and reinforcement measures.

Working condition 2

Calculation results for the typical transient flow velocity distribution at 120 s under working condition 2 in Figure 3(a)–3(c) show the typical flow velocity distribution at section XY over 0–120 s.

Figure 3(a) shows that, during start-up and steady operation of pumps No. 4 and No. 8, the velocity distribution in the inlet pipe and in the elbow of pump No. 4 were similar to those under working condition 1. However, the velocity distribution varied at the junction between the inlet pipe and the main outlet pipe and in pump No. 8's main outlet pipe. Flow velocities in the two inlet pipes were evenly distributed, with the maximum velocity at the elbow and at the junction between the main pipe and pump No. 8's inlet pipe. Multi-level velocities occurred at the elbow. A low-velocity zone of negative pressure occurred at the junction between the inlet pipes and the main pipe, accompanied by disordered backflow. The flow strongly excited the inlet pipe and pump No. 4's main outlet pipe. The flow in pump No. 8's inlet pipe was steady, but compared with

that at the elbow, flow merging in the main pipe was rougher and faster, exerting greater influence on the main pipe than on pump No. 4's inlet pipe. This could cause resistance to the afflux flow at the elbow and increase flow-excited vibration of the elbow and pump No. 4's inlet pipe. Compared with working condition 1, the flow at the main outlet pipe was more unsteady, potentially increasing flow-excited vibration amplitudes.

After pump No. 8 was started with pump No. 4, greater flow excitation of the inlet pipe and pump No. 4's main outlet pipe resulted, requiring reinforcement measures. In contrast, the flow in pump No. 8's inlet pipe was steady with smaller excitation, accordingly. While starting both pumps, unsteady flow can cause strong excitation of the elbow and the main outlet pipe; this is the main cause of pipeline vibration.

Model validation

DASP V10 is a set of multichannel signal acquisition and real-time analysis software developed by the China Orient Institute of Noise & Vibration. In this study, six positions were selected for vibration tests: the water inlet, the elbow, and the junctions between the large and small pipes. DASP V10 should be physically placed as compactly as possible so that it can collect vibration signals simultaneously, ensuring vibration correlation in three directions. To obtain more comprehensive vibration signal data for the pressure pipeline, a three-dimensional coordinate system was established along the radial, axial, and vertical pipeline directions. Three vibration pickups were arranged in a group: two horizontally and one vertically. Since the main pipes of pumps 1–4 in Phase I's second pumping station have similar structures, the layout of the vibration pickups of main pipe No. 4 also applies to pipelines 1–3. For specific arrangements, see Figure 4(c).

This study adopted DASP instrumentation to conduct a field test of vibration characteristics of the No. 1 pressure pipeline under working conditions 1 and 2. DASP uses the so-called method of vibration mode normalization, which represents vibration mode values when the vibration mode of the original admittance point has a value of 1. The acquired vibration mode of the pressure pipeline is displayed with bidirectional trajectories: lines of two colors show vibration trajectories in the structure's upward and downward directions. Vibration mode animations show the dynamic changes of vibration modes of different orders from various angles. This permitted the reliability and validity of the results to be verified. Vibration modes of the first six orders under both working conditions can be obtained by extracting modal information; results are shown in Figure 5.

In working condition 1, when only pump No. 4 operates, its inlet pipe experiences strong vibration along the vertical (Z) direction and a slight torsional vibration along the axial (X) direction. Affected by the operation of pump No. 4, pump No. 8 experiences slight vibration in the X direction, even without starting. The main outlet pipe experiences evident vibration at the No. 2 anchor block.

In working condition 2, when pumps No. 4 and No. 8 operate simultaneously, pump No. 4's inlet pipe shows strong and slight vibrations along the Z and X directions, respectively. Pump No. 8 experiences slight vibration at the main inlet pipe and a small level of vibration at the main outlet pipe along the directions X and Y, especially at the No. 1 and No. 2 anchor blocks.

In summary, flow-excited vibration readily occurred in pump No. 4's inlet and main outlet pipes under both working conditions, and the vibration deformation was clear. Whether pump No. 8 was on or off, its inlet pipe vibrated slightly and had little influence on overall pipeline vibration. Pump No. 4's inlet pipe was more prone to shock and excitation than either its outlet pipe or pump No. 8's inlet pipe. The pipeline's vibration amplitude during normal operation was more apparent than during start-up, indicating more severe pipe vibration during normal operation with a lower level of security. Compared with the main outlet pipe, both inlet pipes vibrated more severely, implying greater safety risks. The field measurement results conform to the simulation results, suggesting that the numerical model is rational and reliable.

Optimized design for vibration attenuation

Pipe diameter

Branch pipe ① and the main pipe were assigned the same diameter. The diameter of branch pipe ② remained unchanged; i.e., the pressure pipeline's diffusion section diameter was reduced but the connection section diameter between the large- and small-diameter pipes was maintained. Repeated trial calculations were conducted for pipe diameters of 1 m to 2 m. Figure 6 shows FLUENT flow simulation velocity contours for pipe diameters of (a) 1 m and (b) 1.4 m.

Figures 6–8 show the FLUENT flow simulation results for optimized design candidates. Compared with working conditions 1 and 2, these designs show steadier pipeline flow and significantly increased velocity. Comparing Figure 6(a) and 6(b), the larger the pipe diameter, the smaller the velocity and the steadier the flow regime. This satisfies the flow calculation formula

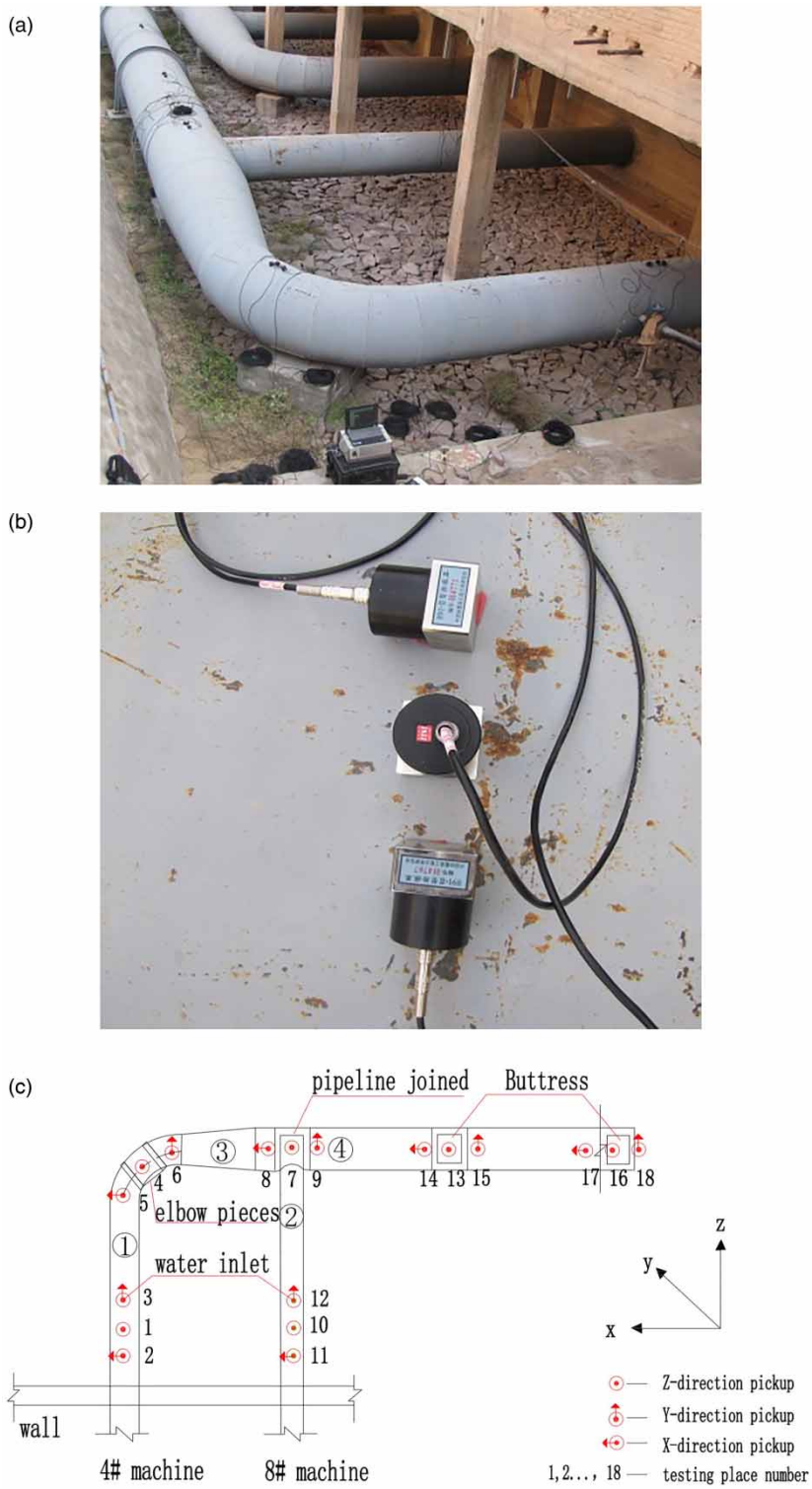

Figure 4 | (a, b) Pick-up site layout and (c) survey point layout.

of $Q = VA$. Therefore, pipeline vibration can be reduced by increasing the pipe diameter. Considered simply from the perspective of pipeline vibration, the larger the pipe diameter, the smaller the pipeline vibration amplitude; however, in actual engineering projects, design complexity, technological limitations, costs, and other factors must also be considered.

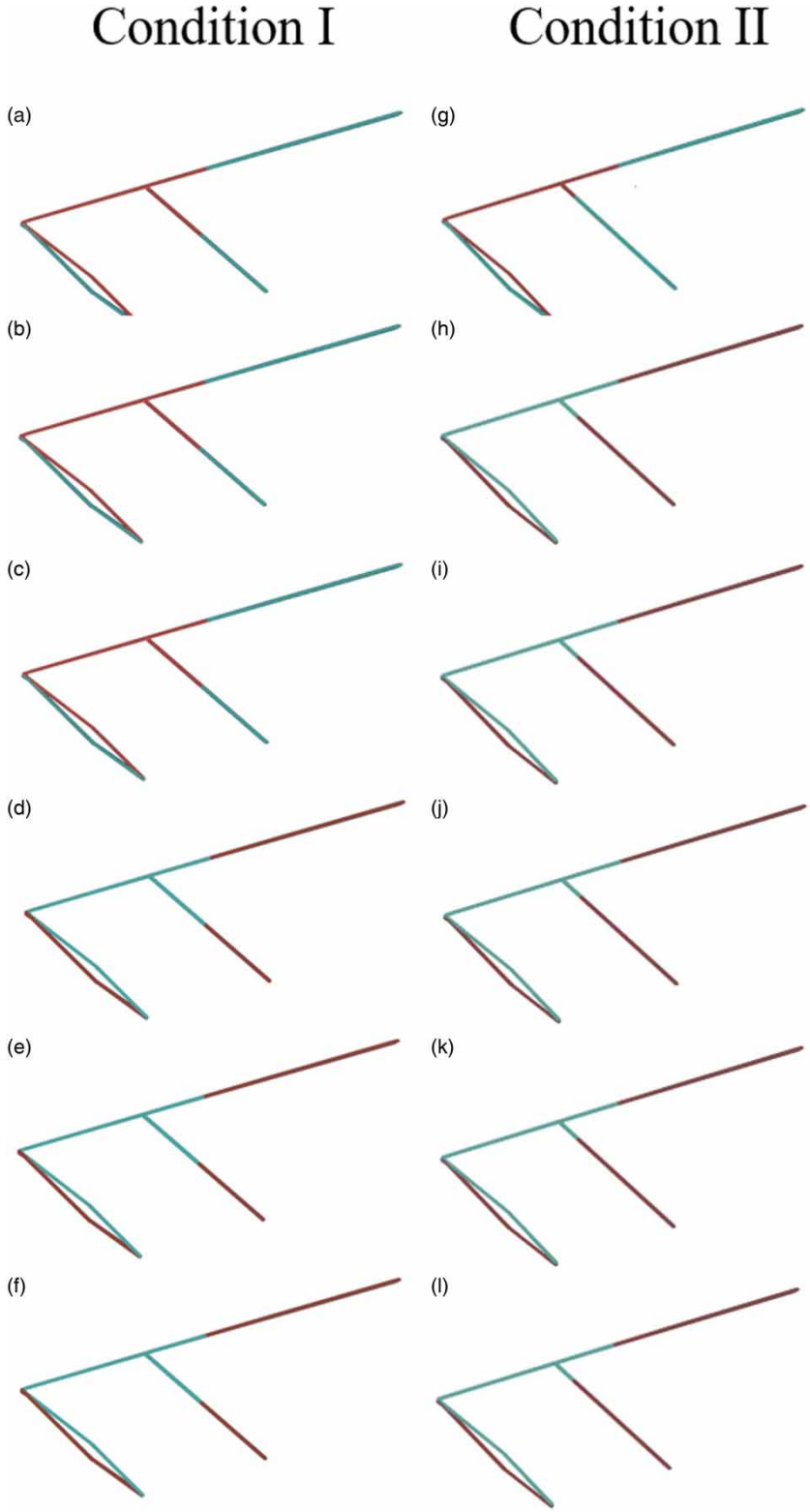

Figure 5 | Vibration mode shapes for working conditions 1 (a–f) and 2 (g–l) in ascending order, beginning with mode 1 (top).

Therefore, using large pipe diameters is not always feasible. With reference to simulation results under both working conditions, the pipe diameter should be 1.4–1.5 m. Additionally, with increased pipe diameter, the flow velocity and pressure intensity both increased, possibly reducing energy loss at the pumping station; therefore, this scheme appears feasible.

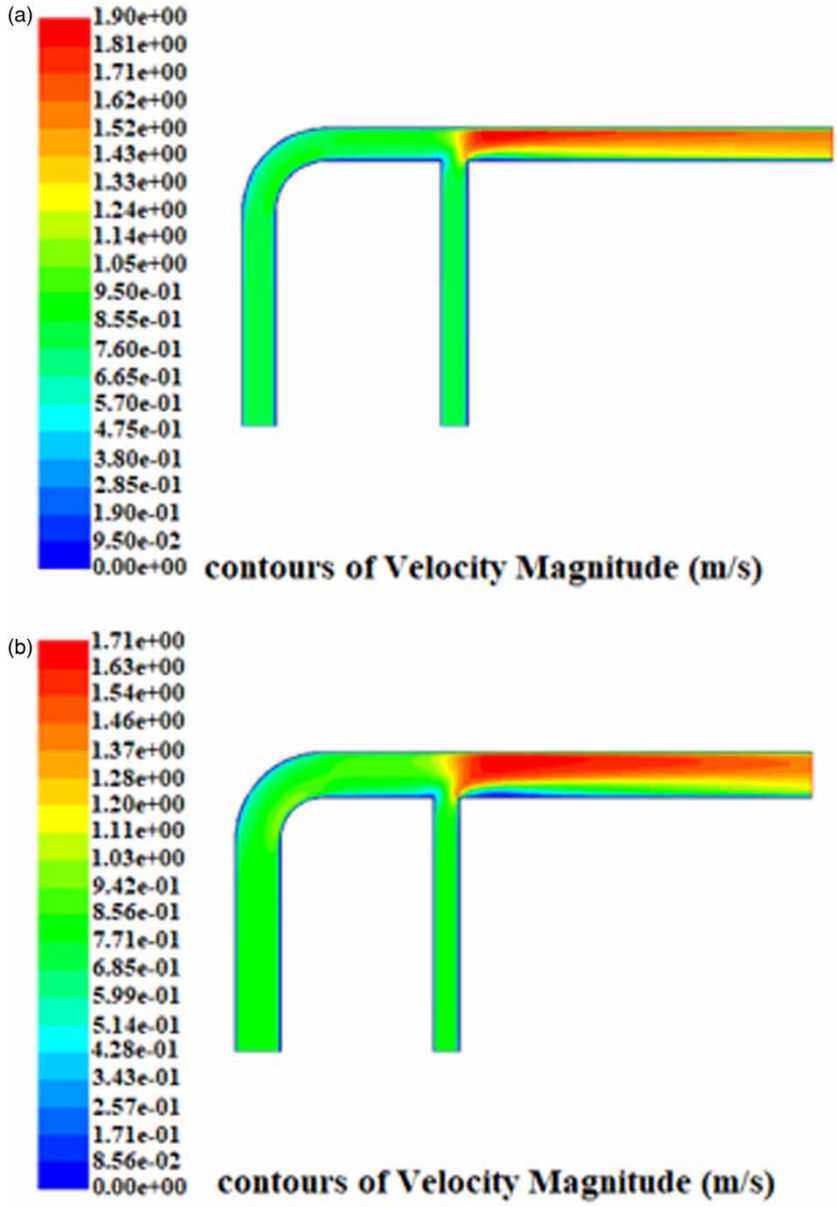

Figure 6 | Flow simulation velocity contours for pipe diameters of (a) 1 m and (b) 1.4 m.

Adjusting the distance between branch pipes

The influence of the distance between branch pipes on the flow regime was considered. Given the plant scale and structure size, after multiple designs and trial calculations based on distances of 1–5 m between branch pipes, the pipeline flow velocity and pressure intensity distributions remained much the same as those in FLUENT's simulations, within the same orders of magnitude. Thus, simply adjusting the distance between two branch pipes has little effect on reducing vibration affects the pumping station's energy loss. The two branch pipes are far apart, and as the flow velocity decreases continually, though at the same order of magnitude, the energy loss increases with distance between the pipes. Details are shown in Figure 7, illustrating the FLUENT simulation's velocity contours for branch pipe separation distance of (a) 2 m and (b) 3 m.

A different approach is to adjust the orientations of the main and branch pipes to achieve a dip angle between the main pipe and the horizontal line. Through adjustment by 1–30°, the flow regime at the elbow and at the joint between the two pipes changed significantly compared with working conditions 1 or 2. The larger the dip angle, the smaller the velocity; therefore,

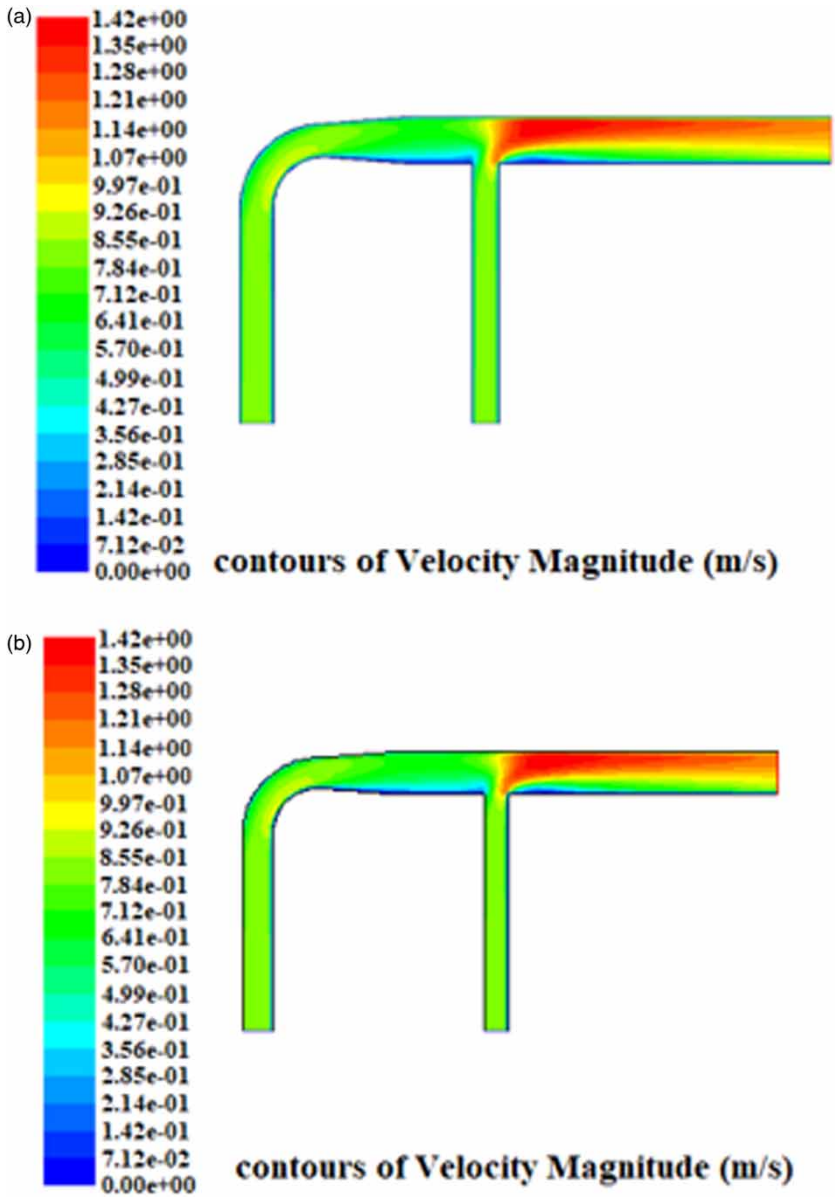

Figure 7 | Flow simulation velocity contours for branch pipe separation distances of (a) 2 m and (b) 3 m.

large dip angles are not always best. Firstly, they make the pipeline harder to process. Secondly, though pipeline vibration is reduced, pumping station energy loss increases, reducing working efficiency. Therefore, this approach is inadvisable. After repeated trials and ignoring possible manufacturing difficulties, it is best to select 2–5°, reducing not only vibration but also pumping station energy loss. The third pumping station in the Yanhuanding Pumping Station Project phase II adopts this pipe layout. Field experiments showed that the resulting vibration intensity is much lower than that of the second pumping station in Phase I. Figure 8 shows FLUENT simulation velocity contours for dip angles of (a) 2° and (b) 20°.

FLUENT flow simulations reveal that, compared with working conditions 1 and 2, adjusting the pipe diameter and the angling the main pipe have significant effects on the flow. In particular, flow regime changes are most evident at the elbow and at the connection between the large and small pipes. In those regions, velocity, which plays a key role in pipeline vibration, increases dramatically. Hence, under hydraulic excitation, pipe diameter and main pipe orientation relative to branch pipes have significant effects on pipeline vibration. In contrast, relative branch pipe locations have little influence on vibration and can be neglected. Another possible remedy is to implement vibration attenuation measures along the pipeline.

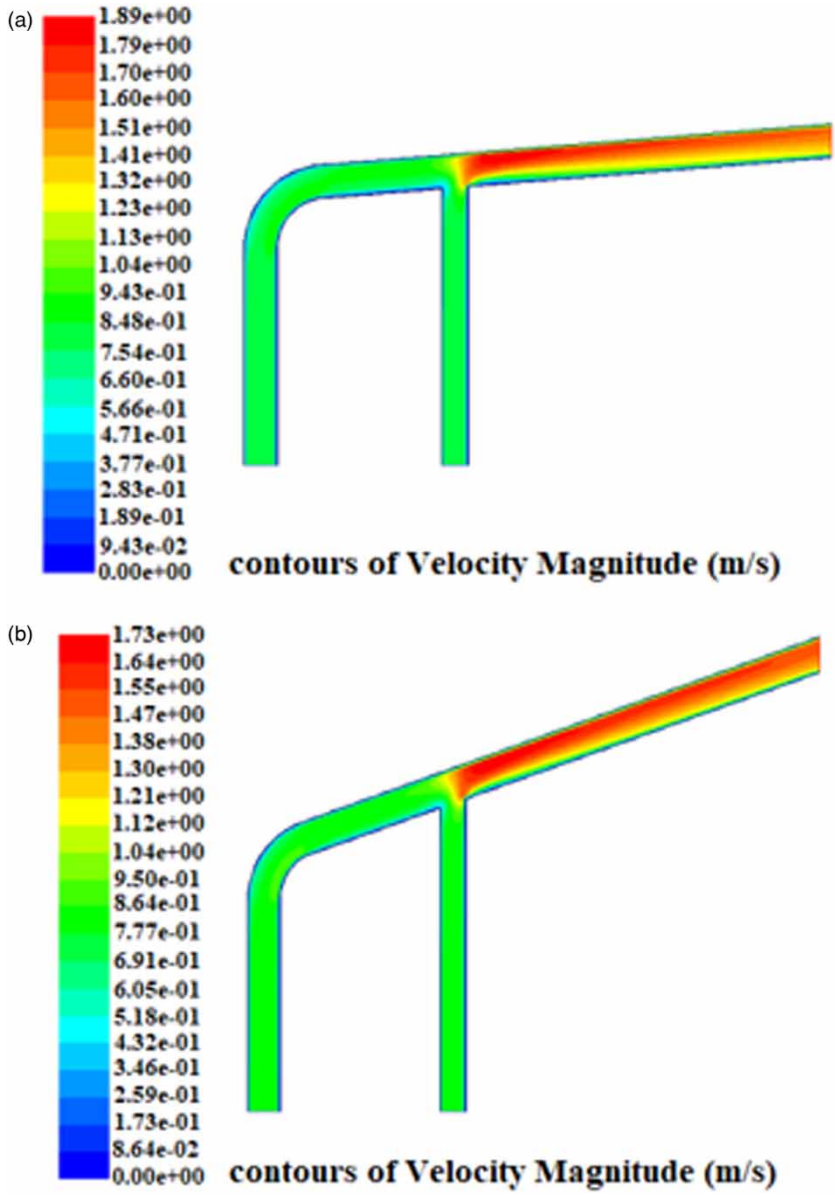

Figure 8 | Flow simulation velocity contours for main pipe dip angles of (a) 2° and (b) 20°.

CONCLUSIONS

This study established an ALGOR-based FSI finite-element model to simulate the characteristics of flow-excited vibration of a pressurized water pipeline at a pumping station. Numerical simulation results were consistent with physical measurements, suggesting that the proposed numerical model is rational and reliable. According to hydrodynamic features and vibration modes under different working conditions, uniformly intense vibration occurs at the inlet pipe, the joint between the main pipe and the branch pipe, and the main outlet pipe. Inlet pipe vibration is more severe than that at the main outlet pipe; this should arouse attention and further verification.

Analysis of the optimized vibration attenuation scheme show that changing the distance between two branch pipes alone has a weak effect on reducing pipeline excitation while increasing pipe diameters and changing the orientation of the main pipe relative to the branch pipes achieve better effects. Ideally, a dip angle of 2–5° reduces not only pipeline vibration but also pumping station energy loss.

The No. 1 pressure pipeline of the second pumping station in the Yanhuanding Pumping Station Project (Phase I) represents a multi-machine, single-pipe station layout. Simulating hydrodynamic characteristics and experimental studies on this pipeline provide both theoretical and practical support for solving vibration problems in similar pressure pipelines and for the safe operation of large-scale pumping stations.

ACKNOWLEDGEMENTS

This work was supported by the National Nature Science Foundation of China (No. 51579102); the University Scientific and Technological Innovation Talents Program of Henan, China (Grant No. 19IRTSTHN030), and the Zhongyuan Science and Technology Innovation Leading Talent Support Program of Henan, China (Grant No. 204200510048). Zhejiang Province Key R&D Program, China (Grant No. 2021C03019). Sincere gratitude is extended to the editor and to the anonymous reviewers for their professional comments which greatly improved the presentation of this paper.

CONFLICTS OF INTEREST

The authors have no conflicts of interest to declare.

DATA AVAILABILITY STATEMENT

All relevant data are included in the paper or its Supplementary Information.

REFERENCES

Ahmadi, A. & Keramat, A. 2010 Investigation of fluid-structure interaction with various types of junction coupling. *Journal of Fluids and Structures* **26**, 1123–1141.

Bu, Y. 2006 *Study on Operating Modal Analysis Method of Pipe System*. Tianjin University of Science and Technology, Tianjin.

Hara, F. 1975 Theory on the two-phase flow induced vibrations. In: Transactions of the 3rd International Conference on Structural Mechanics in Reactor Technology. Paper No. D2/4, London, U.K.

Hara, F. 1980 *Two-Phase Flow-Induced Forces Parametric Vibration in Structural Systems-Pipe and Nuclear Fuel Pins. Report of the Institute of Industrial Science*, Vol. 28. University of Tokyo, Tokyo, pp. 1–43.

Jin, J. D. 1997 Stability and chaotic motions of a restrained pipe conveying fluid. *Journal of Sound and Vibration* **208**, 427–439.

Jin, J. D. & Zou, G. S. 2003 Bifurcations and chaotic motions in the autonomous system of a restrained pipe conveying fluid. *Journal of Sound and Vibration* **260**, 783–805.

Keramat, A. & Ahmadi, A. 2012 Axial vibration of viscoelastic bars using the finite-element method. *Journal of Engineering Mathematics* **77**, 105–117.

Keramat, A., Tijsseling, A. S., Hou, Q. & Ahmadi, A. 2012 Fluid-structure interaction with pipe-wall viscoelasticity during water hammer. *Journal of Fluids and Structures* **28**, 434–455.

Madzivire, G., Maleka, R. M., Tekere, M. & Petrik, L. F. 2019 Cradle to cradle solution to problematic waste materials from mine and coal power station: acid mine drainage, coal fly ash and carbon dioxide. *Journal of Water Process Engineering* **30**, 100474.

Meng, D., Guo, H. Y. & Xu, S. P. 2010 Stability analysis on flow-induced vibation of fluid-conveying pipes. *Journal of Vibration and Shock* **29** (6), 80–83.

Ozdemir, Z., Souli, M. & Fahjan, Y. M. 2010 Application of nonlinear fluid–structure interaction methods to seismic analysis of anch ored and unanchored tanks. *Engineering Structures* **32** (2), 409–423.

Tan, P., Xu, L. & Ling, X. C. 2006 Vibration of water hammer of power pipe system. *Journal of Nanjing University of Science and Technology* **30** (2), 182–185.

Wang, L. 2006 *Stability, Bifurcations and Chaosin Pipes Conveying Fluid*. Huazhong University of Science and Technology, Wuhan.

Wang, X. & Wei, S. H. 2009 Fluid structure coupling vibration analysis of large pumping station Yangtze River. *Yangtze River* **40** (22), 56–59.

Xie, Q. & Xue, S. T. 2006 A hybrid algorithm for optimal sensor placement of structural health monitoring. *Journal of Tongji University (Natural Science)* **34** (6), 726–731.

Zanganeh, R., Ahmadi, A. & Keramat, A. 2015 Fluid-structure interaction with viscoelastic support effects during waterhammer. *Journal of Fluids and Structures* **54**, 215–234.

Zeng, G. H. 2007 *Research on Nonlinear Yibratian Model and Simulation of Fluid-Conveying Pipes*. Wuhan University of Science and Technology, Wuhan (in Chinese).

First received 18 March 2021; accepted in revised form 29 June 2021. Available online 12 July 2021